

# Influence of Pulse Electrodeposition and Heat Treatment on Microstructure, Tribological, and Corrosion Behavior of Nano-Grain Size Co-W Coatings

Somayeh Abazari, Saeed Rastegari, and Shahram Kheirandish

(Submitted December 7, 2016; in revised form March 31, 2017; published online May 30, 2017)

In the present study, Co-W nano-structured alloy coatings are produced on low-carbon steel substrate by means of pulse electrodeposition from a citrate-based bath under different average current densities and duty cycles. The results indicate that the coating deposited under 60% of duty cycle and 1 A/dm<sup>2</sup> of average current density exhibit optimum pulse plating conditions with 44.38 wt.% W, 37 nm grain size, and 758 HV microhardness. The effect of heat treatment temperature on microstructure, composition, corrosion behavior, and morphology of amorphous deposited Co-W alloy with 44 wt.% W was investigated. The microhardness of the coating increased to 1052 HV after heat treatment at 600 °C, which is due to the formation of Co<sub>3</sub>W and CoWO<sub>4</sub> phases in the deposit. Furthermore, the coatings heat-treated at 600 °C had lower friction coefficients and better wear resistance under various loads than before heating.

**Keywords** Co-W coating, corrosion, duty cycle, electrodeposition, heat treatment, wear resistance

## 1. Introduction

Electrodeposited chrome coatings with high hardness and appropriate abrasive properties have been used in a wide range of applications to prevent surface detriments, and also these coatings have catalytic activity (Ref 1). However, environmental protection rules have become effective in restricting the use of hexavalent chromium due to the high toxicity of Cr(VI) (Ref 2). Therefore, Ni- and Co-based alloys are applied for abrasive applications as a substitute for Cr. Among available coatings, electrodeposition of W with iron group metals together have a high melting point and are often considered as superalloys or high-performance alloys. The Co-W alloy coating has attracted more attention due to its higher hardness, smooth surface, wear resistance, corrosion resistance, and acceptable magnetic properties (Ref 3-7). These alloys are deposited using direct and pulse electric currents (PEDs). PED processes with optimized pulse parameters often provide advantages such as the smaller size of grains and smoother surface of coatings that improves the wear and corrosion resistance of alloys (Ref 8-10). Nucleation control and grain refinement lead to the preparation of unique composition and microstructure of the deposit (Ref 11). Several researchers have successfully investigated pulse electrodeposition of Co-W coatings by

citrate electrolyte (Ref 12-17). Shtefan et al. studied the influence of pulse frequency on microstructure and microhardness of Co-W alloys and the effect of pulse parameters on tungsten content and electrochemical behavior of Co-W alloys (Ref 18). Tsyntsaru et al. investigated the effect of composition on the corrosion resistance of electrolytic Co-W coatings deposited with various current densities (Ref 19). Likewise, in some other studies, the influence of organic additives and heat treatment, optimizing the parameters of the deposition to obtain coatings which have properties similar to chrome plating, is investigated (Ref 20-23). Weston et al. demonstrated that the wear resistance of the Co-W alloy coating was better than that of electrodeposited chromium under certain sliding conditions (Ref 24). Fenghua et al. found that wear resistance varies by hardness values at higher forces, but it is under the influence of morphology, surface roughness, and hardness of lower forces. At higher amounts of nodules, the number of contact points increases at the surface, which causes the higher friction coefficient and lower wear resistance of the coating (Ref 25). One of the properties of alloys deposited using PED is a thermodynamically unstable microstructure in which high microstructure energy is a driving force for recrystallization during annealing. Heat treatment influences the structure, present phases and crystallites of the coating that leads to variation in alloy properties such as microhardness, wear and corrosion behavior (Ref 26, 27).

Some studies have investigated the effect of heat treatment on microstructure of Co-W and Ni-W electrodeposits (Ref 28, 29), and the change in hardness of these coatings, with respect to aging conditions, is well documented; for example, plated Co-W coatings electrodeposited from acidic baths with a grain size between 220 and 450 nm (Ref 30). After a thermal treatment of such coatings at 400 °C, the grain size reduces down to 80 nm and the deposits become compact and dense. In addition, the microhardness of heat-treated coatings at 100 up to 400 °C for 4 h increases from 600 to 880 VHN. On extending the heat treatment at 400 °C, the as-plated homoge-

Somayeh Abazari and Saeed Rastegari, Shahram Kheirandish, School of Metallurgy and Materials Engineering, Iran University of Science and Technology, Narmak, Tehran 1684613114, Iran. Contact e-mails: abazari@metaleng.iust.ac.ir, somayeh.abazari@gmail.com, rastegari@iust.ac.ir, and kheirandish@iust.ac.ir.

neous phase decomposes into a variety of crystalline phases including Co<sub>7</sub>W {216} and Co<sub>3</sub>W {002} (Ref 31).

The aim of the present study is to find the relationship between both pulse electrodeposition parameters duty cycle and current density and composition (relative percentages of tungsten and cobalt), phase homogeneity (amorphous, crystalline, or mixed), and surface microstructure of the prepared Co-W nano-crystalline alloys. Moreover, the effects of heat treatment temperatures on tribology and corrosion properties of amorphous electrodeposited alloys are studied, which are seldom investigated on coatings produced by PED.

## 2. Materials and Methods

All samples were prepared using PED under a galvanostatic condition in a citrate bath containing (mol/l): CoSO<sub>4</sub>·7H<sub>2</sub>O—0.2; Na<sub>2</sub>WO<sub>4</sub>·2H<sub>2</sub>O—0.2; C<sub>6</sub>H<sub>8</sub>O<sub>7</sub>—0.04; Na<sub>3</sub>C<sub>6</sub>H<sub>5</sub>O<sub>7</sub>·2H<sub>2</sub>O—0.25; C<sub>6</sub>H<sub>8</sub>O<sub>7</sub>—0.04 and H<sub>3</sub>BO<sub>3</sub>—0.65. The pH was adjusted by boric acid. Sodium citrate was used as the complexing agent. The anode (mild steel) and cathode (Pt mesh) were cut in 4 × 3.5 cm and 3 × 3 cm dimensions, respectively. The steel substrates were mechanically grounded to a 0.1-0.15 micron surface finish with SiC abrasive papers. It was degreased in an alkaline solution (NaOH 10 wt.%) at 70 °C for 15 min, rinsed in distilled water, activated in an acidic solution (HCl 10 vol.%) for 1 min, rinsed in distilled water again, and then immersed in the plating bath. The plating process was performed in various average current densities and duty cycles with variations in on and off times (Table 1). In the case of the plating process, a pulse rectifier device (RCTP50V50A) was used. Surface morphology and chemical composition of alloys were confirmed using scanning electron microscopy (VEGA. TESCAN) equipped with EDS. Phase investigations were performed using XRD (Philips X'pert, PW3040/60) in which Cu-K<sub>α</sub> radiation of 1.54 Å was operated at 30 kV and 30 mA. Scherrer's equation was used to demonstrate the mean grain size:

$$d = \frac{0.9\lambda}{\beta \cos \theta} \quad (\text{Eq 1})$$

where  $d$  is mean grain size (nm),  $\lambda$  is wavelength (1.54 Å),  $\beta$  is full width at half maximum height (in radians), and  $\theta$  is peak position (Ref 18). The microhardness measurements of samples were performed using Vickers microhardness device (SCTMC-MHV-10002) on the cross section of each coated substrate (10 s under a 25 gr load). The results are reported by an average of five different points.

**Table 1 Plating parameters used for electrodeposition**

Parameters	value
CoSO <sub>4</sub> ·7H <sub>2</sub> O, (mol/L)	0.2
pH	6.7 ± 0.1
Temperature, (°C)	60 ± 2
Rotating rate, (rpm)	150
Deposition time, (h)	2
Pulse frequency, (Hz)	200
Duty cycle, (%)	20, 40, 60, 80
Average current density, (A/dm <sup>2</sup> )	1, 2, 4, 6

For investigating the effect of heat treatment on coatings, all samples were sealed in a quartz tube under vacuum atmosphere for 4 h at 200-600 °C with the rate of 5 °C/min and then cooled inside the furnace. For wear behavior characterization, a pin-on-disk test was used according to ASTM G99-05 was used which the pin was a hardened AISI 52100 steel that used in distance of 300 m and applied a load of 7, 15, and 30 N standard at room temperature. A corrosion test was performed using the potentiostat/galvanostat system (IVIUMSTAT) in 3.5 wt.% NaCl solution. Polarization measurement was performed using sweeping potential from open circuit potential at the scan rate of 1 mV/s.

### 2.1 Effect of Duty Cycle

SEM image (Fig. 1a) confirmed that, in the duty cycle of 20%, the coating surface consisted of fine pyramids. By increasing in the duty cycle, the size of the pyramid is decreased where at the duty cycle of 80%, the morphology is spherical with flat grains (Fig. 1b). Also, when the duty cycle is improved, 'on-time' increases during plating, which results in grain growth. There should be an equilibrium between 'on-time' and 'off-time.' 'On-time' should be short enough to prevent the controlled deposition with diffusion. In addition, 'off-time' must be long that ions transferring from the electrolyte to the double layer are completed. Figure 2 confirms that W content in the deposit increases between 20 and 60% duty cycle and then decreases at 80%.

With increasing 'on-time' to 60% duty cycle, overpotential of deposition increases and causes more W content on the coating. With more increase in duty cycle, the effect of lower 'off-time' overcomes 'on-time' increasing. Therefore, a number of ions weight percent, containing complexing agent, decrease in either the diffusion layer or subsequently in the deposition (Fig. 2).

Figure 3 illustrates that Co-W solid solution is the main phase of all duty cycles. As can be clearly, duty cycles have an influence on the orientations of deposition crystallography. In the duty cycle of 20%, the (101) plane is the main crystallographic direction, while with increasing duty cycle, main crystallographic orientation is (100). Grain sizes increase as a result of increasing the duty cycle. The average current density ( $I_A$ ), in pulse electrodeposition is given by:

$$I_A = \text{peak current } (I_p) \times \text{duty cycle } (\gamma) \quad (\text{Eq 2})$$

And the nucleation rate ( $\vartheta$ ) is as given:

$$\vartheta = k_1 \exp\left(-\frac{k_2}{|\eta|}\right) \quad (\text{Eq 3})$$

where  $k_1$  is proportionality constant,  $k_2$  is the amount of energy needed for nucleation, and  $\eta$  is crystallization overpotential. From Eq 3, it can be inferred that, as increased duty cycle at constant  $I_A$ , peak current density ( $I_p$ ) decreased; So, the overpotential and nucleation rate decreased resulting in coarser crystals (Ref 32).

Nano-crystalline strengthening obtained thorough making a solid solution and grain boundary strengthening. Alloying element resist in high temperature like W causes a significant increase in hardness of nano-crystallographic deposits. Figure 2 indicates that increase in deposit hardness and increase in W content are in agreement. The microhardness values of samples

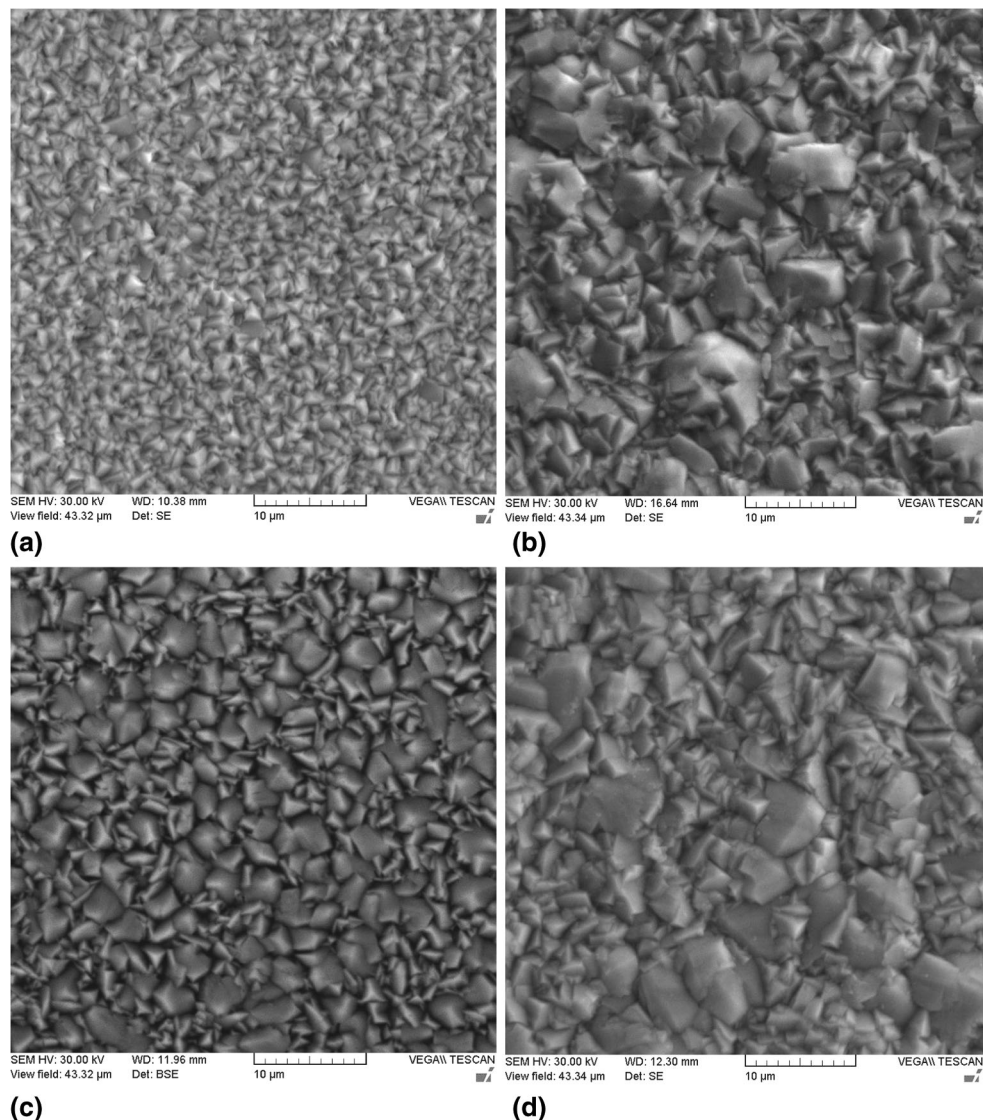


**Fig. 1** Surface morphology of Co-W deposit for different duty cycles of (a) 20%, (b) 40%, (c) 60%, and (d) 80%

in duty cycle between 20 and 60% are more than in the duty cycle of 80% (Fig. 2). It confirms that grain boundary strengthening is obtained due to a decrease in grain size and also more deposit W content, comparing with duty cycle 80% which has lowest W content and highest grain size.

## 2.2 Effect of Current Density

SEM images of deposits at different current densities (Fig. 4) confirm that surface morphology is influenced significantly by the current density. With increasing current density, the morphology of deposits changes from fine pyramids to the nodular type. When the current density increased, a great proportion of applied current will be used for hydrogen reduction reactions, which leads to coarse nodules and fine structure of deposits (Ref 33). The W content increases with an increase in current density and current peak enhancement (Fig. 5). At higher current densities (6 A/dm<sup>2</sup>), cathodic potential shifts to more negative values; So increasing in the surface diffusion of complex ions, containing W, will occur at the cathode surface (Ref 33, 34). Therefore, the W content of coatings increases.

The main constituent phase at the current density of 1 and 2 A/dm<sup>2</sup> (Fig. 6) is Co(W) solid solution. XRD patterns confirm that the Co-W morphology becomes amorphous with increasing the current density to 4 and 6 A/dm<sup>2</sup> (Fig. 6).

Generally, crystalline or amorphous phase formations during electrodeposition of binary alloys are described by W content of deposit or overpotential of the electrode. Overpotential enhancement leads to higher nucleation rates and finer grains formation (Ref 19). At a constant duty cycle, overpotential is measured by the current density peak. Increase in average current density increases the current density peak; So, the overpotential of electrode rises and causes a deposit with a random distribution of atoms on the cathode surface, which results in the formation of an amorphous coating (Ref 20). An amorphous deposit forms at 4 A/dm<sup>2</sup> and higher current densities.

Microhardness of deposit values decreases by increasing current density and grain size (Fig. 5). Formation of amorphous structure in the deposit, at current densities higher than 4 A/dm<sup>2</sup>, causes the decrease in the coating microhardness values. Besides, the morphology of deposits at higher current densities is coarser and rougher due to the reduction of hydrogen; thus,

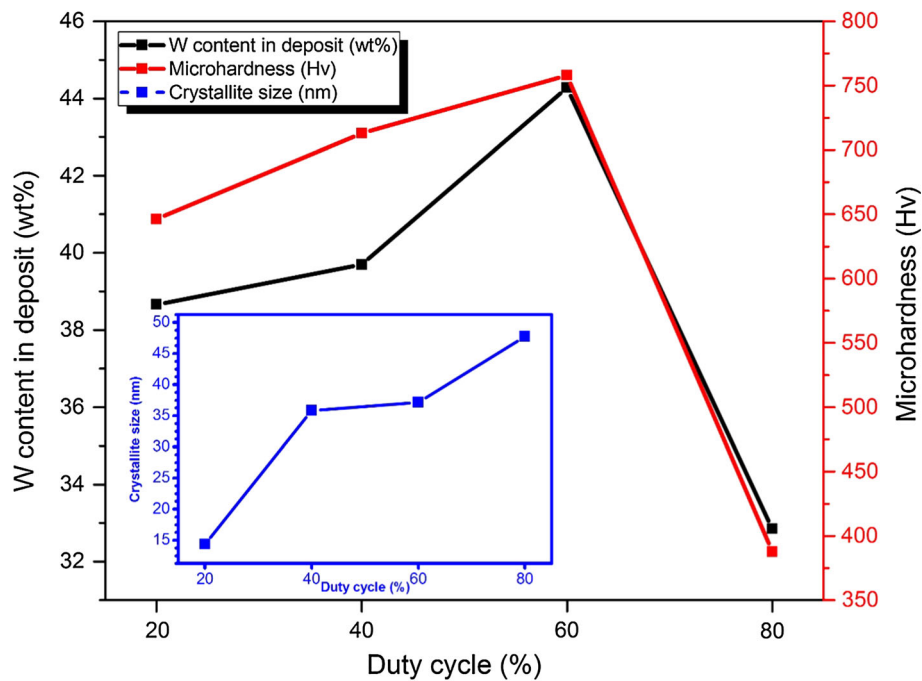


**Fig. 2** The content of W, microhardness, and grain size of Co-W deposit as a function of different duty cycles (average current density of 1 A/dm<sup>2</sup>, frequency 200 HZ)

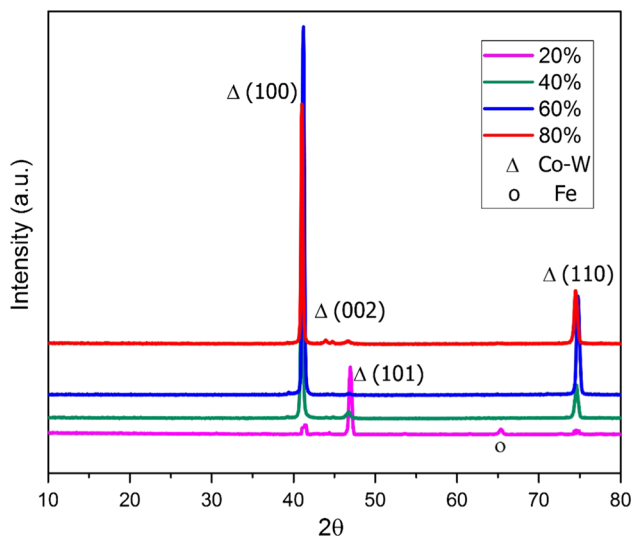


**Fig. 3** Deposit XRD patterns for different duty cycles (average current density of 1 A/dm<sup>2</sup>, frequency 200 Hz)

microhardness values decrease. Images of electron microscopy (BSE) and the line scan of elements from the cross section of the Co-W coating resulted from electroplating with an average current density of 4 A/dm<sup>2</sup> and duty cycle of 20% and the frequency of 200 Hz are shown in Fig. 7. As can be seen, the distribution of elements in the coating is quite uniform. The coating has a smooth and uniform interface with the steel substrate and average thickness of 23 microns.

### 2.3 Heat Treatment Effect on Microstructure and Characteristics of Coating

With the rise of heat treatment temperature, the amorphous deposit proceeds to crystalline structure (Fig. 8). At 600 °C,

polycrystalline structure and grain size of 41 nm are obtained. Generally, the formation of crystalline or amorphous structures during electrodeposition of Co-W is described by W content values or electrode overpotential. By increasing overpotential, the nucleation rate rises and a coating with fine grains is deposited. With heat treatment, enough thermal energy is provided for the penetration of Co and W atoms into the deposit volume in atomic scale. Thus, the formation of intermetallic and nano-crystalline of Co<sub>3</sub>W occurs (Ref 18). The Co-W system shows the presence of two intermediate phases, Co<sub>7</sub>W<sub>6</sub> and Co<sub>3</sub>W (Ref 35). when the amount of tungsten is lower than 55 wt.% Co<sub>3</sub>W and CO(W) can be formed. Based on the phase diagram of Co-W, the formation of the Co<sub>3</sub>W in this temperature is possible. CoWO<sub>4</sub> is also observed based on JCPDS- 015-0867 reference card, which is the result of residual oxygen in the quartz tube. Because necessary activation energy for extraction of oxygen from the surface is too high, the oxide composition which is formed through adsorption of oxygen by W on the surface remains stable up to 700 °C (Ref 21). At 400 °C, the orientation of deposit in (200) direction is stronger, while at the temperature of 600 °C, the preferred direction is (002). (002) direction is perpendicular to the alloy deposit growth plane, so it is the favorite direction for deposition on the substrate. According to Fig. 9, heat treatment leads microhardness of the deposit to increase from 426 to 1059 HV.

Coordination of formed compound and structure phases could overcome the reduction in microhardness which was decreased by grain growth. Thus, microhardness of the heat-treated Co-W alloy at 600 °C is more than the value reported for hard-chrome coatings (848 HV) (Ref 17).

Figure 10 demonstrates morphology of Co-W coatings after heat treatment deposited at a current density of 4 A/dm<sup>2</sup> containing 23.5 wt.% W. The as-deposited coating had an amorphous structure with nodular morphology (Fig. 4c). As can be seen clearly, by increasing the temperature to 400 and

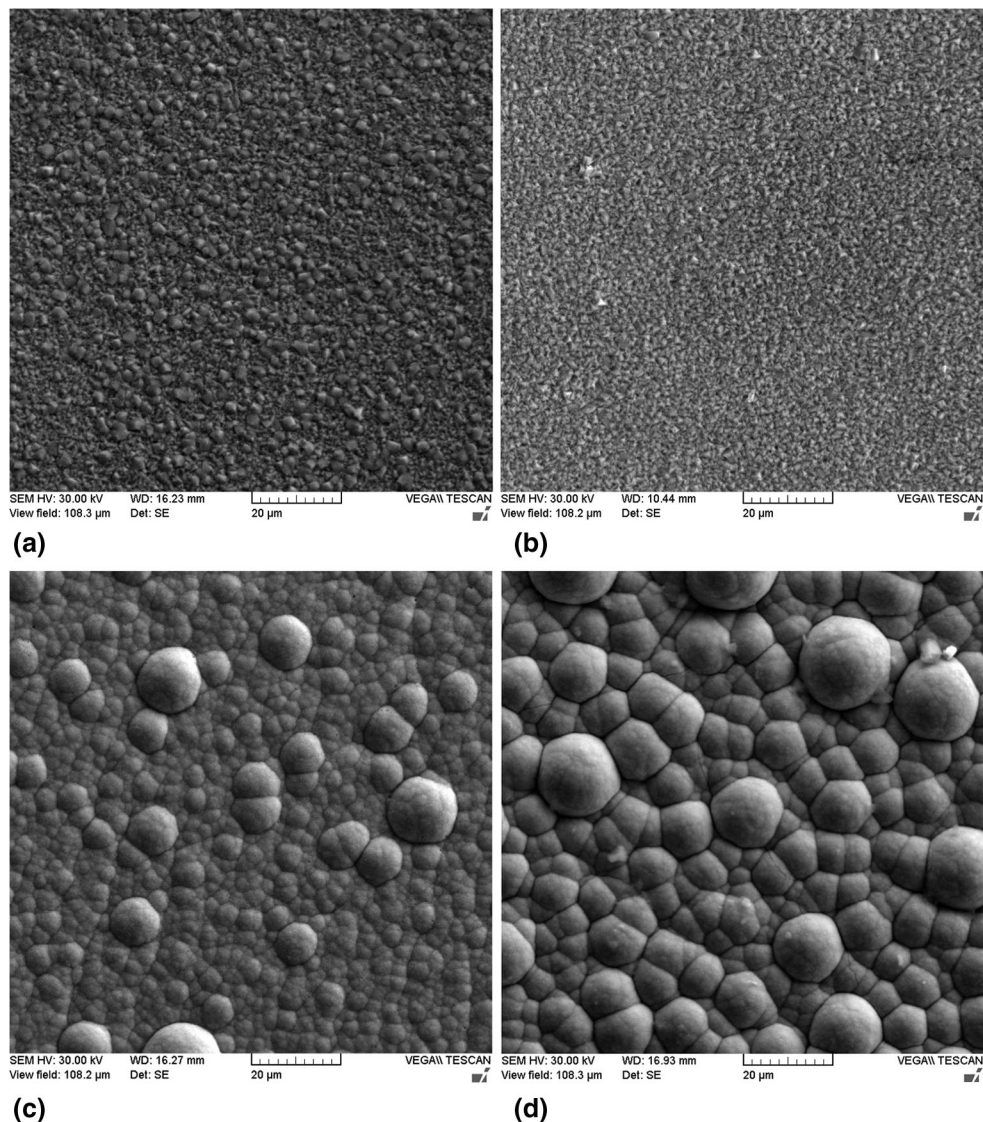


**Fig. 4** Surface morphology of Co-W deposits processed with duty cycle of 20%, average current density of (a) 1 A/dm<sup>2</sup>, (b) 2 A/dm<sup>2</sup>, (c) 4 A/dm<sup>2</sup> and (d) 6 A/dm<sup>2</sup>

500 °C, nodules grew immensely and conjugated to each other. Each of these nodules consists of many crystallites. Chen and Singh et al. reported that probably there is the formation of the vitriform zone and decrease in alloy melting point for electrodeposited Co-W coatings (Ref 22) There is a high possibility to form a vitriform zone for Co-W alloy containing 20 wt.% or more W.

#### 2.4 Corrosion Behavior Measurement

Results represented in Table 2 and Fig. 11 confirm an improvement in the corrosion resistance of Co-W deposited alloy compared to the steel substrate after heat treatment. The lowest corrosion current and corrosion rate were related to heat-treated sample at 400 °C. Coating treated at 600 °C also had a lower corrosion current and corrosion rate than the as-deposited alloy coating. Therefore, because of low corrosion current and rate, it can be concluded that corrosion resistance of Co-W alloy coatings has improved after heat treatment.

Grain boundaries influence the electrochemical behavior of the surface in two ways: First, they are high energetic sites,

which preferentially react in the presence of corrosive media. Second, more grain boundaries resulted in the low cathode-to-anode ratio that is an effective agent in the accentuation of localized corrosion, and guided the corrosion into the substrate, so corrosion resistance improved (Ref 19). The penetration of the outside elements is done faster in nano-crystalline materials due to the higher volume fraction of grain boundaries and a higher rate of penetration along them. Therefore, the protective oxide layer is formed faster in these materials and uniformity and density of passive film improves and leads to increase in corrosion resistance of the coating (Ref 18). The microcracks are filled with this protective layer, and their negative effect is eliminated in exacerbating the corrosion. The high density of grain boundaries in nano-crystalline materials will significantly affect corrosion behavior. W is more resistive against corrosion and increases corrosion resistivity (Ref 8). Nano-crystalline alloy coatings of Ni-W and Ni-Fe-W have special corrosion resistance due to preferential decomposition of Ni and formation of W on the coating surface. In the presence of corrosive media, W transfers to the surface and forms a protective passive

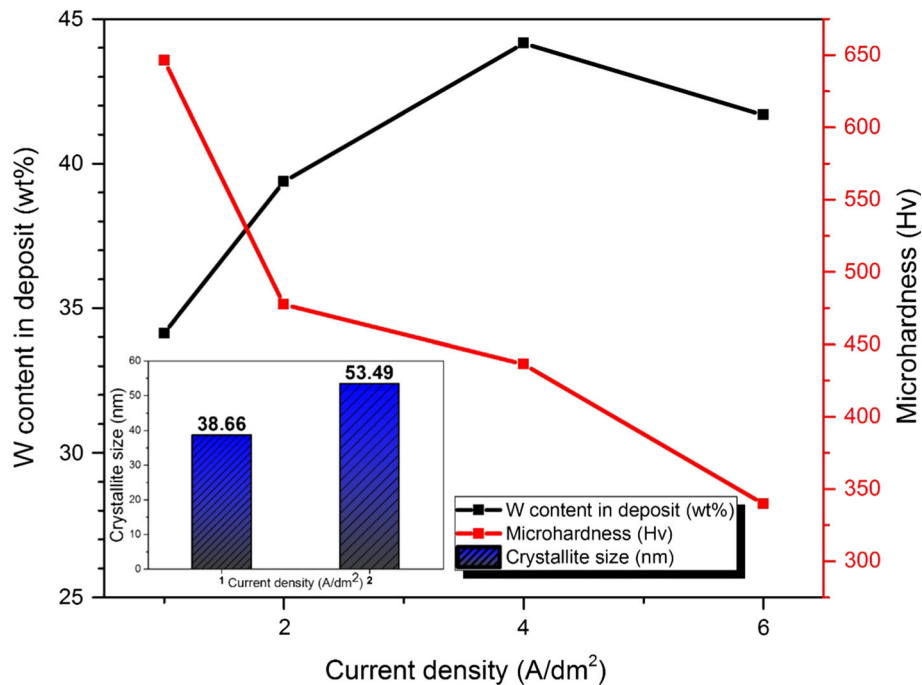


**Fig. 5** Content of W content in deposit, microhardness values, and grain size of the coatings as a function of average current density (duty cycle of 20%, frequency of 200 Hz)

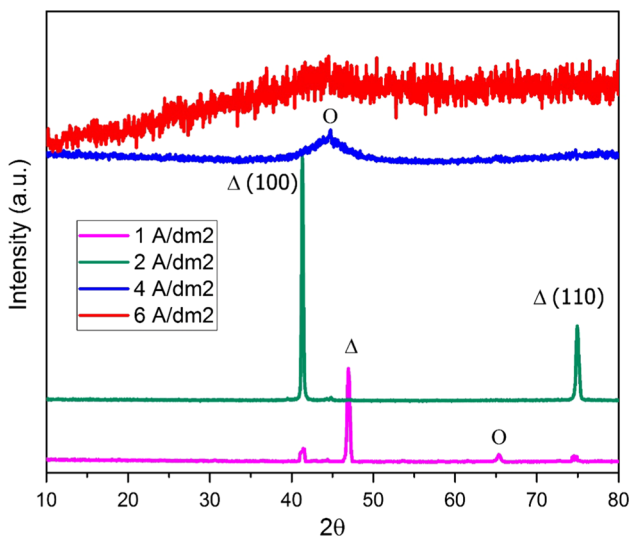


**Fig. 6** XRD patterns of the deposits with different average current densities (duty cycle of 20%)

film (Ref 22). Higher polarization resistance is related to  $\text{Co}_3\text{W}$  compound formation due to heat treatment (Ref 23). In the treated coatings, W was distributed regularly compared to the amorphous coating on which W was randomly distributed, so an improvement in the corrosion resistance was observed.

The coating heat-treated at 600 °C has a larger surface morphology and higher surface roughness than at 400 °C, which leads to less corrosion resistance in comparison with heat treatment at 400 °C, and a heat-treated coating at 600 °C has coarse grains and lower grain boundary; it seems that uniform attack occurred due to the reduction of grain boundaries.

## 2.5 Wear Test Results

Wear behavior of deposited alloys before and after heat treatment was investigated under various loads. Wear rate and friction coefficient of coatings as a function of applied load are represented in Fig. 12. These results were related to alloys deposited under a current density of 4 A/dm<sup>2</sup>, the duty cycle of 20%, which has the microhardness value of 436 HV. Then, heat treatment was performed at 600 °C. Heat treatment at this temperature leads to microhardness enhancement to 1095 HV which improved wear characteristic of the Co-W coating. Increasing the applied load results in more stress at the contact point, which also increases the real contact. It leads to more weight loss of the coating and friction coefficient enhancement (Ref 18, 36). As it can be observed in Fig. 12, by increasing the applied load, as the pin penetrates in more depth, the wear rate of the coating increases too. Similarly, the friction coefficient of the as-deposited alloy at the applied load of 15 N decreases from 0.63 to 0.46 after heat treatment. Increase in of wear resistance of heat-treated samples was the result of added microhardness, which prevented peeling of the deposit and deformation during pin movements. Because of lower wear rates, friction coefficient decreased due to the lower contact area between the pin and deposit. In fact, hardness and wear resistance improved significantly due to the formation of  $\text{Co}_3\text{W}$  and homogenization of the deposit after heat treatment which promotes the grain refining and precipitation strengthening effect.

Figure 13(a) is related to the Co-W as-deposited alloy, and peeling can be observed on the surface. After heat treatment of deposits, lower peelings and flat nodules are drawn in the wear direction as shown in Fig. 13(b). Wear lines are viewable on the nodules. Deformed materials as a result of peeling of the coating surface are placed between the nodules. Nodules

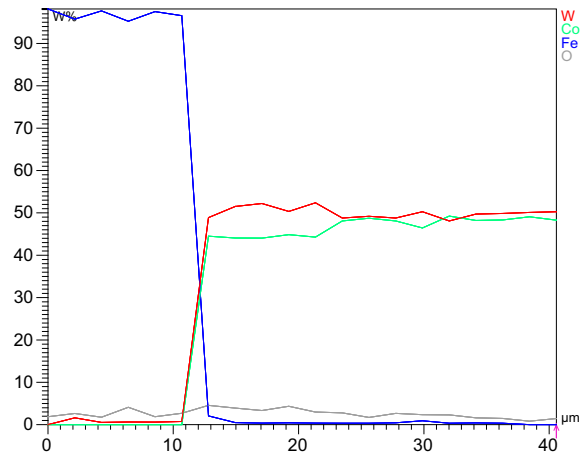
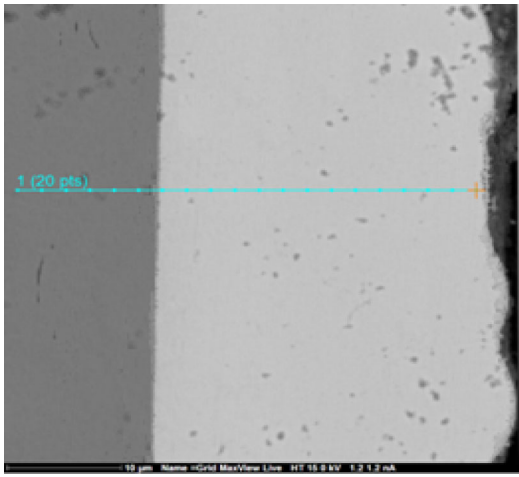


**Fig. 7** Cross-sectional morphology and line scan of Co-W coating with an average current density of 4 A/dm<sup>2</sup> and duty cycle of 20%, and the frequency of 200 Hz

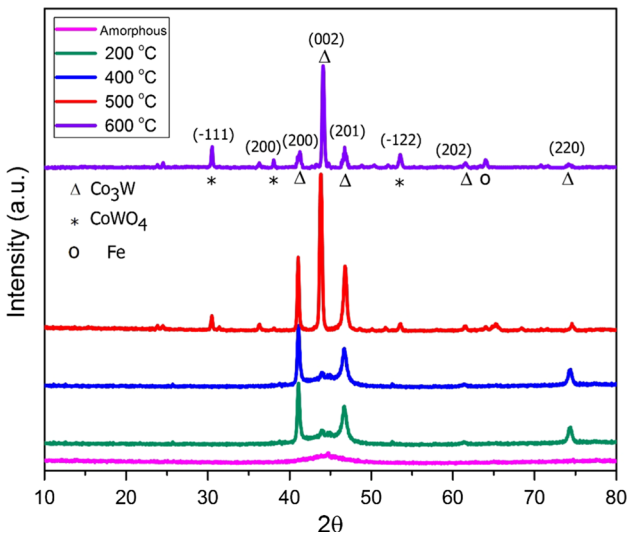


**Fig. 8** XRD patterns of the deposits with an average current density of 4 A/dm<sup>2</sup> and the duty cycle of 20%, heat-treated at different temperatures

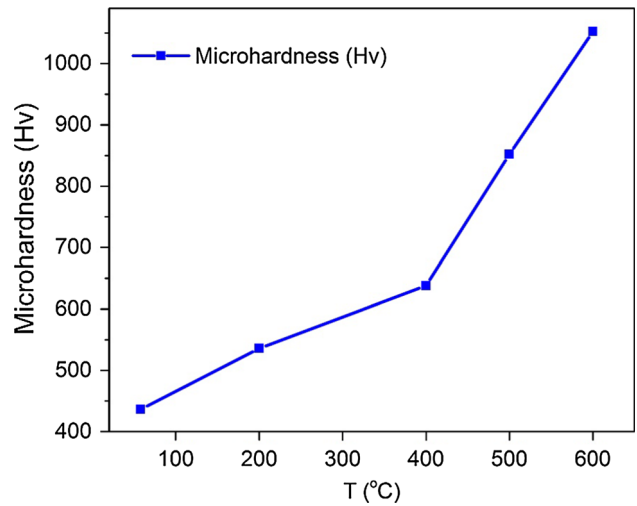


**Fig. 9** Effect of heat treatment temperature on microhardness of Co-W deposit (average current density of 4 A/dm<sup>2</sup> and the duty cycle of 20%)

existing on the plated surface coating prior to heat treatment lead to increased tension acts at contact points that subsequently increase friction coefficient. The domain mechanism of wear in Fig. 13(a) is adhesive wear, while it is adhesive-abrasive wear in Fig. 13(b). During test performance, the coating plastically deformed due to poor resistance against shear loads. Wear layers are observed at the wear impact point. These wear layers become hard worked as a result of constant pin movement. So, cracks have initiated and propagated easily at these layers and finally led to peeling of that layer.

Figure 13(c), and (d) is related to the wear surface of coatings before and after heat treatment at the applied load of 30 N. Clearly, increasing the applied load intensified the peeling volume. The wear surface has more cracks. More peelings in the wear direction increased the friction coefficient. Figure 13(d) indicates that compared to as-deposited coatings (Fig. 13c), peelings reduced and cracks grew more slowly.

High toughness of the treated samples in comparison with as-deposited alloy coatings results in a lack of cracks and fractures, while in as-deposited coatings, microhardness is lower which leads to plastic deformation and hard strengthening resulting in an intensive adhesion between the pin and coating surface. The main mechanism for both coatings (Fig. 13c, and d) is adhesive wear.

An increase in the hardness of the coating with increased wear resistance and reduced weight loss resulted by the wear process due to a simultaneous reduction in shear strength of the coating also leads to a reduction of the friction coefficient. Friction coefficient has an important role in interpreting tribological results. Therefore, the plot of moment changes of the friction coefficient in Co-W alloy coatings before and after heat treatment is provided at applied load of 7 N in Fig. 14. Fewer fluctuation changes in the plot of the heated treatment friction coefficient in comparison with the coating prior to heat treatment indicate deformation and less wear debris during the

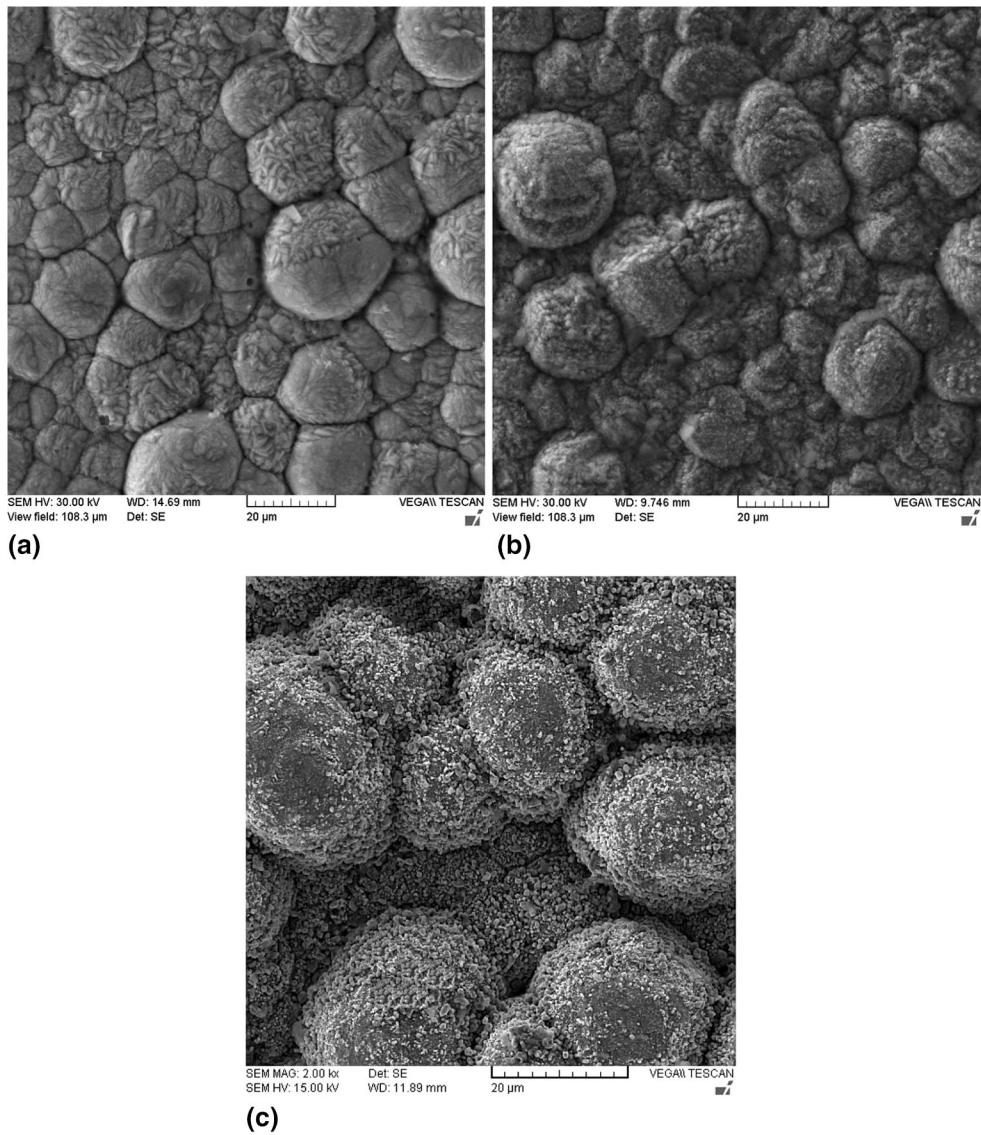


**Fig. 10** Surface morphology of Co-W coatings with an average current density of 4 A/dm<sup>2</sup>, frequency of 200 Hz, and the duty cycle of 20%, heat-treated at (a) 200 °C (b) 400 °C, and (c) 500 °C

**Table 2** Extracted parameters from E vs. log i plot in Fig. 11

Coating	$I_{corr}$ (A/cm <sup>2</sup> )	$E_{corr}$ (V vs. Ag/ AgCl)	C.R, (mpy)	$R_p$ , (ohm)
As-plated	$7.3 \times 10^{-5}$	-0.667	0.506	$2.52 \times 10^3$
Heat-treated at 400 °C	$0.306 \times 10^{-5}$	-0.864	0.212	$7.41 \times 10^3$
Heat-treated at 600 °C	$5.29 \times 10^{-5}$	-0.573	0.363	$1.31 \times 10^3$
Steel	$8.98 \times 10^{-5}$	-0.484	0.622	$1.27 \times 10^3$

wear process and better confirm wear resistance of these coatings. High friction coefficient with high fluctuations in coatings before heat treatment represents avulsion of the coating and significant deformation of the surface in the wear process of these coatings. In addition, increasing friction coefficient is related to the placement of more wear debris on wear path.

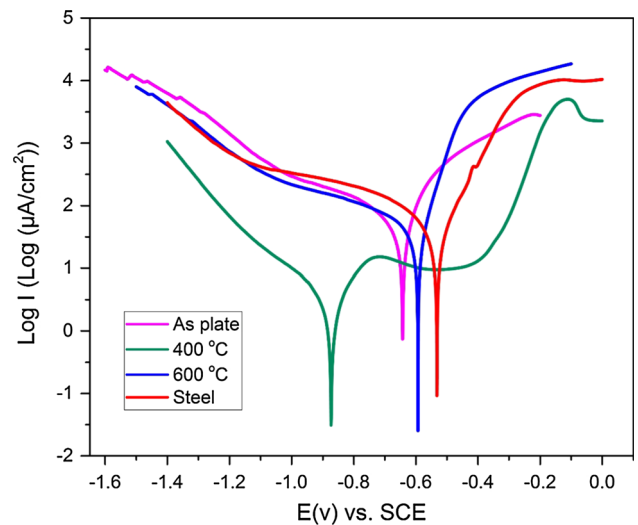


**Fig. 11** Log I vs. E plots



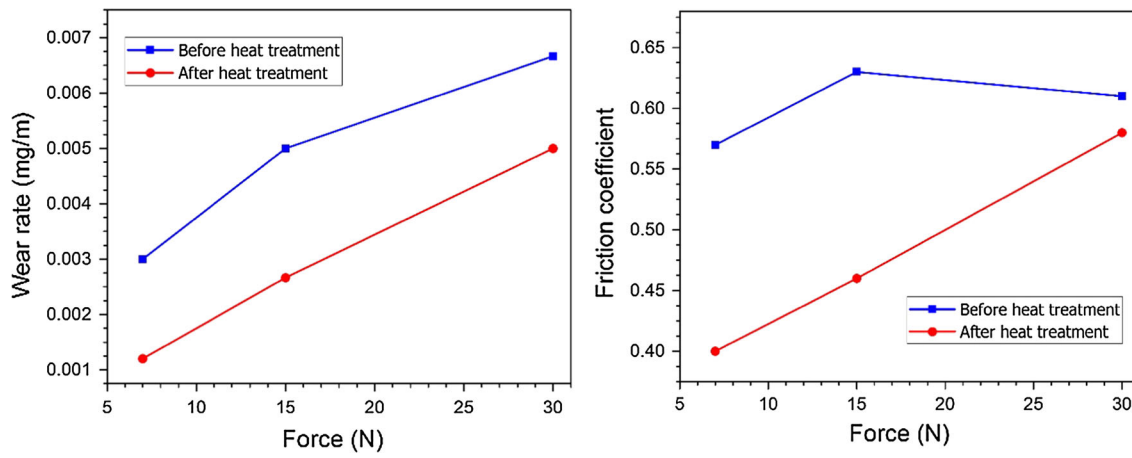


**Fig. 12** Wear rate and friction coefficient of Co-W alloy coatings before and after heat treatment at 600 °C as a function of applied load

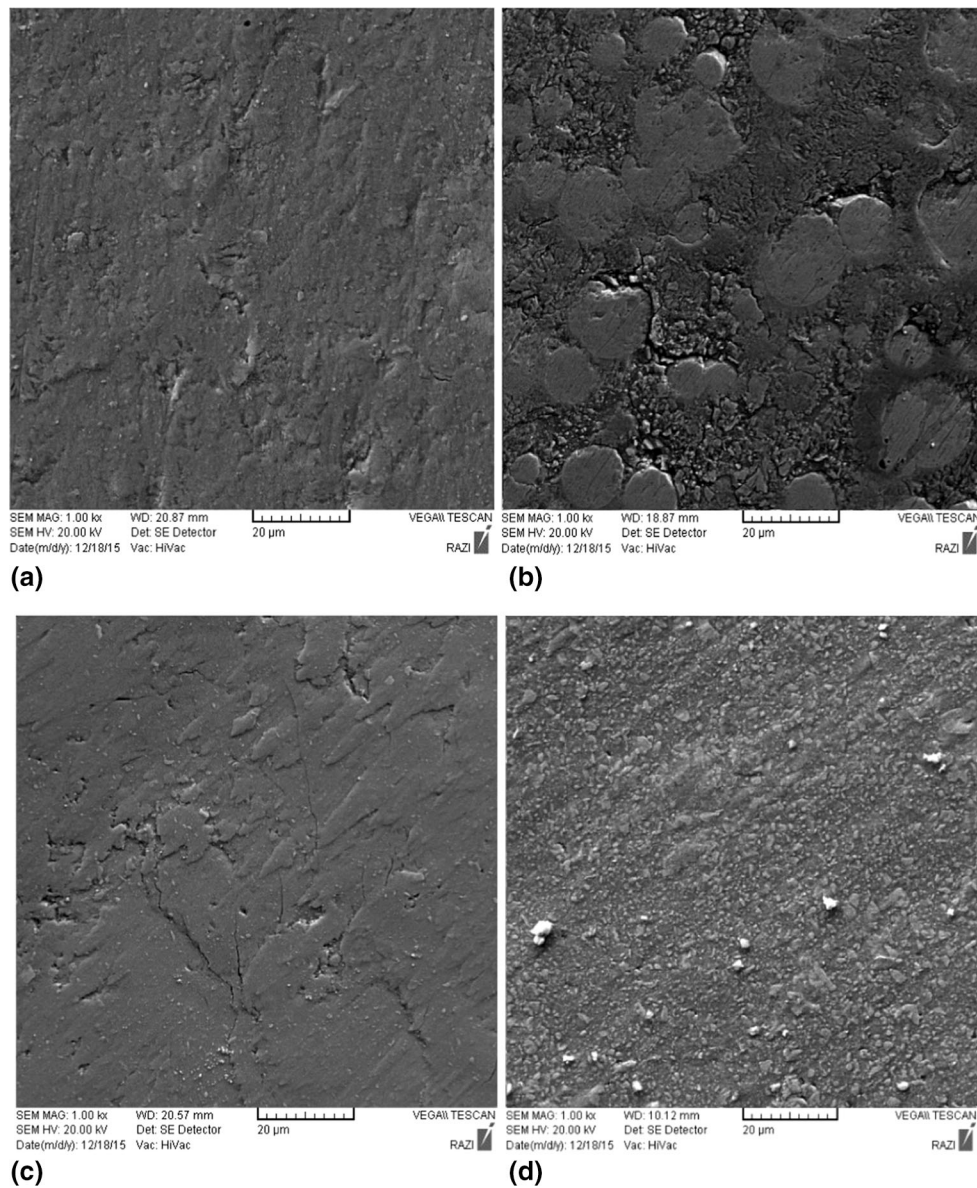


**Fig. 13** SEM images of the worn surface of Co-W alloy coatings before and after heat treatment at applied load of 15 N (a,b) and 30 N (c,d), respectively

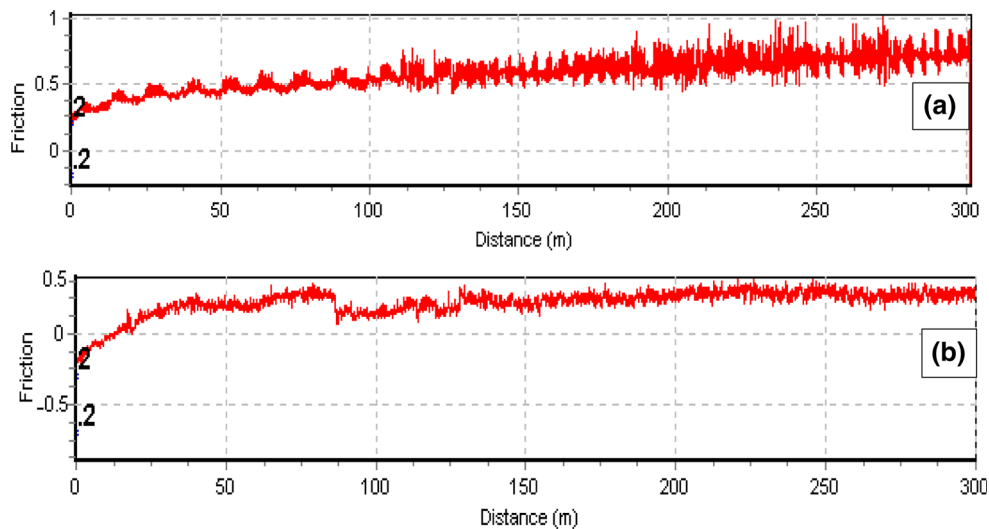


**Fig. 14** The friction coefficient of Co-W coatings (a) before and (b) after heat treatment at 600 °C at an applied load of 7 N

### 3. Conclusions

The present study tries to describe the effect of parameters on the Co-W deposits. The current density was known as the most important possible variable to make amorphous or crystalline deposits. Increase in current density up to 4 A/dm<sup>2</sup> makes coatings structure amorphous. The hardness of the coating rises with decreasing in grain size and enhancement in the W content of the deposit. Also, increasing heat treatment temperature converts the amorphous coating to crystalline and also leads to the formation of different phases (Co<sub>3</sub>W and CoWO<sub>4</sub>) and crystal orientations. Microhardness of the coating increases significantly by increasing the heat treatment temperature (from 436 to 1059 HV at 600 °C). Due to significant microhardness value and formation of the Co<sub>3</sub>W phase in heat-treated deposit at 600 °C, lower friction coefficient and better wear resistance under different loads comparing with deposit without treatment are observed. The results also confirm that corrosion resistance of the coating was improved by heat treatment. The coating treated at 400 °C exhibited minimum corrosion rate.

### References

1. P. Żabiński, K. Mech, and R. Kowalik, Electro-catalytically Active Co-W and Co-W-C Alloys Electrodeposited in a Magnetic Field, *Electrochim. Acta*, 2013, **104**, p 542–548
2. EUR-Lex - 32002L0095 - EN. Off J L 037, 13/02/2003 P 0019 - 0023; 2003
3. T. Nasu, M. Sakurai, T. Kamiyama, T. Usuki, O. Uemura, K. Tokumitsu et al., Structural Comparison of M-W (M = Fe, Ni) Alloys Produced by Electrodeposition and Mechanical Alloying, *Mater. Sci. Eng. A*, 2004, **375–377**, p 163–170
4. C.N. Tharamani, P. Beera, V. Jayaram, N.S. Begum, and S.M. Mayanna, Studies on Electrodeposition of Fe-W Alloys for Fuel Cell Applications, *Appl. Surf. Sci.*, 2006, **253(4)**, p 2031–2037
5. K.R. Sriraman, S. Ganesh Sundara Raman, and S.K. Seshadri, Synthesis and Evaluation of Hardness and Sliding Wear Resistance of Electrodeposited Nanocrystalline Ni-W Alloys, *Mater. Sci. Eng. A*, 2006, **418(1–2)**, p 303–311
6. C.N. Panagopoulos, V.D. Papachristos, and L.W. Christoffersen, Lubricated sliding Wear Behaviour of Ni-P-W Multilayered Alloy Coatings Produced by Pulse Plating, *Thin Solid Films*, 2000, **366(1–2)**, p 155–163
7. E. Edward Anand and S. Natarajan, Effect of Carbon Nanotubes on Corrosion and Tribological Properties of Pulse-Electrodeposited Co-W Composite Coatings, *J. Mater. Eng. Perform.*, 2015, **24(1)**, p 128–135
8. M. Mulukutla, V.K. Kommineni, and S.P. Harimkar, Pulsed Electrodeposition of Co-W Amorphous and Crystalline Coatings, *Appl. Surf. Sci.*, 2012, **258(7)**, p 2886–2893
9. E.W. Brooman, Wear Behavior of Environmentally Acceptable Alternatives to Chromium Coatings: Cobalt-Based and Other Coatings, *Met. Finish.*, 2004, **102(10)**, p 42–54
10. L. Elias, K. Scott, and A.C. Hegde, Electrolytic Synthesis and Characterization of Electrocatalytic Ni-W Alloy, *J. Mater. Eng. Perform.*, 2015, **24(11)**, p 4182–4191
11. Lou HH and Huang Y. Electroplating. In: Encyclopedia of Chemical Processing. 2006. p. 839–848
12. N. Tsyntsaru, A. Dikumar, H. Cesiulis, J.-P. Celis, Z. Bobanova, S. Sidel'nikova et al., Tribological and Corrosive Characteristics of Electrochemical Coatings Based on Cobalt and Iron Superalloys, *Powder Metall. Met. Ceram.*, 2009, **48(7–8)**, p 419–428
13. V.V. Shtefan, M.V. Ved, M.D. Sakhnenko, L.V. Pomoshnyk, and L.P. Fomina, Regularities of the Deposition of Cobalt-Tungsten Alloys by Pulsed Currents, *Mater. Sci.*, 2007, **43(3)**, p 429–433
14. D.Z. Grabco, I.A. Dikumar, V.I. Petrenko, E.E. Harea, and O.A. Shikimaka, Micromechanical Properties of Co-W Alloys Electrodeposited Under Pulse Conditions, *Surf. Eng. Appl. Electrochem.*, 2007, **43(1)**, p 11–17
15. L. Wang, Y. Gao, T. Xu, and Q. Xue, A Comparative Study on the Tribological Behavior of Nanocrystalline Nickel and Cobalt Coatings Correlated with Grain Size and Phase Structure, *Mater. Chem. Phys.*, 2006, **99(1)**, p 96–103
16. M.A.M. Ibrahim, S.S. Abd El Rehim, and S.O. Moussa, Electrodeposition of Noncrystalline Cobalt-Tungsten Alloys from Citrate Electrolytes, *J. Appl. Electrochem.*, 2003, **33(7)**, p 627–633
17. H. Capel, P.H. Shipway, and S.J. Harris, Sliding Wear Behaviour of Electrodeposited Cobalt-Tungsten and Cobalt-Tungsten-Iron Alloys, *Wear*, 2003, **255(7–12)**, p 917–923
18. F. Su, C. Liu, and P. Huang, Friction and Wear of Nanocrystalline Co and Co-W Alloy Coatings Produced by Pulse Reverse Electrodeposition, *Wear*, 2013, **300(1–2)**, p 114–125
19. Z. Ghaferi, K. Raeissi, M.A. Golozar, A. Saatchi, and S. Kabi, Comparison of Electrodeposition Aspects and Characteristics of Ni-W and Co-W Alloy Nanocrystalline Coatings, *Iran J. Mater. Sci. Eng.*, 2010, **7(4)**, p 16–24
20. P. Bera, H. Seenivasan, K.S. Rajam, and V.K. William Grips, XRD, FESEM and XPS Studies on Heat Treated Co-W Electrodeposits, *Mater. Lett.*, 2012, **76**, p 103–105
21. N. Tsyntsaru, H. Cesiulis, A. Budreika, X. Ye, R. Juskenas, and J.-P. Celis, The Effect of Electrodeposition Conditions and Post-Annealing

- on Nanostructure of Co-W Coatings, *Surf. Coat. Technol.*, 2012, **206**(19–20), p 4262–4269
22. D.P. Weston, S.P.A. Gill, M. Fay, S.J. Harris, G.N. Yap, D. Zhang et al., Nano-Structure of Co-W Alloy Electrodeposited from Gluconate Bath, *Surf. Coat. Technol.*, 2013, **236**, p 75–83
  23. H. Jin, S.M.S.I. Dulal, C. Burm, and C.-K. Kim, Electrochimica Acta Characterisation of Electrodeposited Co-W-P Amorphous Coatings on Carbon Steel, *Electrochim. Acta*, 2008, **54**(2), p 370–375
  24. D.P. Weston, S.J. Harris, P.H. Shipway, N.J. Weston, and G.N. Yap, Establishing Relationships Between Bath Chemistry, Electrodeposition and Microstructure of Co-W Alloy Coatings Produced from a Gluconate Bath, *Electrochim. Acta*, 2010, **55**(20), p 5695–5708
  25. F. Su, C. Liu, and P. Huang, Establishing Relationships Between Electrodeposition Techniques, Microstructure and Properties of Nanocrystalline Co-W Alloy Coatings, *J. Alloys Compd.*, 2013, **557**, p 228–238
  26. A.V. Boltushkin, V.G. Shadrow, V.M. Fedosyuk, and S.S. Grabchikow, Heat-Treatment Effect on Structure and Magnetic Properties of Hard Magnetic Co-W Films for Perpendicular Magnetic Recording, *Czechoslov. J. Phys.*, 1988, **38**(10), p 1174–1176
  27. M. Zeinali-Rad, S.R. Allahkaram, and S. Mahdavi, Effect of pH, Surfactant, and Heat Treatment on Morphology, Structure, and Hardness of Electrodeposited Co-P Coatings, *J. Mater. Eng. Perform.*, 2015, **24**(9), p 3209–3217
  28. S. Eskin, O. Berkh, G. Rogalsky, and J. Zahavi, Co-W Alloys for Replacement of Conventional Hard Chromium, *Plat. Surf. Finish.*, 1998, **85**(4), p 79–84
  29. V.M. Fedosyuk and J.M. Riveiro, Crystallization of Single-Layered and Multilayered Amorphous Co-W Films, *J. Non Cryst. Solids*, 1992, **143**, p 153–156
  30. H.Z. Abdel, Electrodeposition of Cobalt-Tungsten Alloys from Acidic Bath Containing Cationic Surfactants, *Mater. Lett.*, 2003, **57**(16–17), p 2558–2564
  31. C.L. Aravinda, V.S. Muralidharan, and S.M. Mayanna, Electrodeposition and Dissolution of Co-W Alloy Films, *J. Appl. Electrochem.*, 2000, **30**(5), p 601–606
  32. M.S. Chandrasekar and M. Pushpavanam, Pulse and Pulse Reverse Plating-Conceptual, Advantages and Applications, *Electrochim. Acta*, 2008, **53**, p 3313–3322
  33. R. Juškėnas, I. Valsiūnas, V. Pakštas, A. Selskis, V. Jasulaitienė, V. Karpavičienė et al., XRD, XPS and AFM Studies of the Unknown Phase Formed on the Surface During Electrodeposition of Ni-W Alloy, *Appl. Surf. Sci.*, 2006, **253**(3), p 1435–1442
  34. S.M.S.I. Dulal, H.J. Yun, C.B. Shin, and C.-K. Kim, Electrodeposition of CoWP Film, *Electrochim. Acta*, 2007, **53**(2), p 934–943
  35. K.P. Gupta, The Co-Cr-W (Cobalt-Chromium-Tungsten) System, Phase Equilibria and Diffusion, *Phase Equilib. Diffus.*, 2006, **27**, p 178–183
  36. D.P. Weston, P.H. Shipway, S.J. Harris, and M.K. Cheng, Friction and Sliding Wear Behaviour of Electrodeposited Cobalt and Cobalt-Tungsten Alloy Coatings for Replacement of Electrodeposited Chromium, *Wear*, 2009, **267**(5–8), p 934–943